J. Fluid Mech. (1982), *vol.* 117, *pp.* 91–106
Printed in Great Britain

Phase-distribution mechanisms in turbulent low-quality two-phase flow in a circular pipe

By D. A. DREW AND R. T. LAHEY
Rensselaer Polytechnic Institute, Troy, New York 12181, U.S.A.

(Received 29 October 1979 and in revised form 4 November 1981)

The radial distribution of the volumetric vapour (or void) fraction in steady, fully developed turbulent two-phase flow is described for vertical low-quality bubbly flows in a circular pipe. The analysis is based on the phasic equations of conservation of momentum in the axial and radial directions. Mixing-length theory is used to model the turbulent stresses in the continuous phase. The predicted flow structure shows three distinct regions. The 'outer' region, that is, the region away from the wall and the centre-line, has a uniform void distribution. For upflow, a bubble layer is predicted near the wall, while for downflow, vapour coring is predicted, with a peak in void fraction at the centre-line. These predictions are in agreement with observed void profiles.

1. Introduction

Two-phase flows are of great practical concern in a large number of engineering disciplines, including the chemical, petroleum, and power industries. As an example, questions concerning nuclear-reactor safety have led to a demand for an understanding of the detailed phase-distribution mechanisms involved in two-phase flows.

The complexity of two-phase situations is reflected in the type of experimental data available. Most of the two-phase data consists of global measurements, such as total static pressure drop and quality. Engineering design and analysis are based largely on empirical correlations, which are usually valid only for the specific geometries and flow conditions tested. When more detailed information is needed, such as the lateral void distributions, the correlations fail to provide any insight or information.

The purpose of this paper is to provide a rigorous mechanistic basis for the description of radial void distributions in a circular pipe for low-quality bubbly flow. By providing a fuller understanding of the process involved in this simple geometry, it is hoped that more understanding can be gained of similar phenomena in complex geometries, so that correlations can eventually be replaced by analytical models.

Detailed measurements of many time-averaged, local properties of vertical, co-current adiabatic air-water upflow in a circular pipe were taken by Serizawa (1974). Figure 1 shows the void distribution obtained for a given superficial liquid velocity j_L. For low-quality flow, Serizawa observed that the flow was bubbly, and that a pronounced bubble layer occurred near the wall. As the quality increased, the flow made a transition to slug flow. For these flows, the void fraction showed a peak in the centre of the pipe.

Other data, taken by Oshinowo & Charles (1974) showed quite different trends for

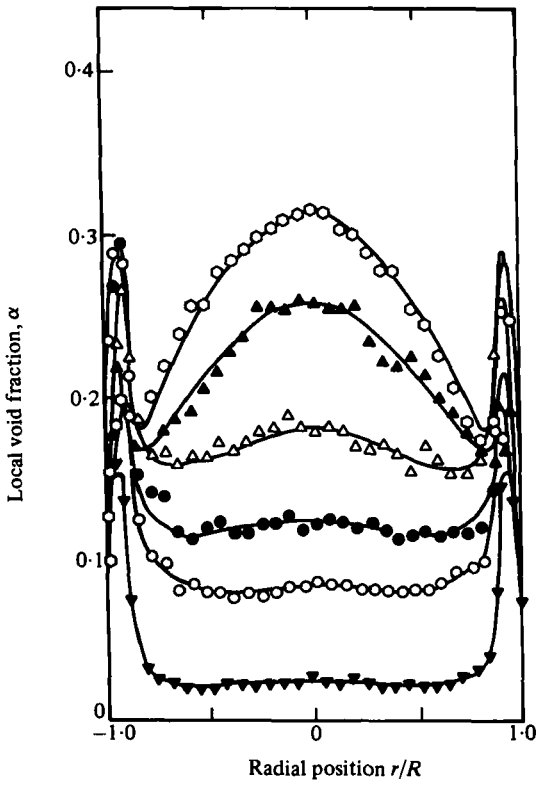

FIGURE 1. Void fraction $\alpha(r)$; profiles for j_L = 1·03 m/s (Serizawa 1974), Z/D = 30. Bubble flow: ▼, flow quality 0·0085; ○, 0·0170; ●, 0·0258; △, 0·0341. Slug flow: ▲, 0·0427; ○, 0·0511.

vertical co-current downflow. In particular, there was no bubble layer at the wall, but there was pronounced tendency for the bubbles to concentrate along the centre-line of the pipe ('coring'). An accurate model of phase distribution should predict these observed trends.

In what follows, we shall derive equations that predict the velocity and void profiles in bubbly flow in a circular pipe. Our analysis is based on the time-averaged equations of motion for multidimensional two-phase flows. These equations are applied to steady, fully developed air–water two-phase flow in a circular pipe. Two fundamental assumptions will be made concerning the turbulent stresses, namely that: (i) the gas-velocity fluctuations are driven by the velocity fluctuations in the liquid, and (ii) the liquid Reynolds stresses are adequately modelled using mixing-length theory. The cross-sectional area divides naturally into three regions. In the wall boundary layer, the viscous stresses, the turbulent stresses and the buoyancy forces all combine to determine the void and the velocity profiles. Close to the centre-line, classical mixing-length theory underestimates the effect of the turbulence. Thus, there must be a region near the centre-line where the Reynolds stresses, modelled using mixing-length theory, must be modified. Finally, in the rest of the cross-section, the viscous forces are negligible, and standard mixing-length theory is expected to give good results.

2. Averaged equations

Perhaps the most practical approach to multidimensional two-phase flows is based on time-averaging. While there are difficulties with the simplest time-averaging process, more sophisticated averaging processes do not lead to new insights into the fundamentals of two-phase flow, nor do they lead to averaged equations that are different in any way, other than in the interpretation of the averaged variables. Thus the most simple definition of time averaging will be used here, and, as has become customary, the associated difficulties will be ignored.

The time average, as defined by Delhaye (1968) and expounded upon by Ishii (1975), is defined by

$$\bar{f}(\mathbf{x},t) = \frac{1}{T}\int_{t}^{t+T} f(\mathbf{x},t')\,dt'. \tag{1}$$

The characteristic function of phase k is defined by

$$X_k(\mathbf{x},t) = \begin{cases} 1 & \text{if } \mathbf{x} \text{ lies in phase-}k \text{ at time } t, \\ 0 & \text{otherwise.} \end{cases} \tag{2}$$

The time fraction of phase k is defined to be $\alpha_k = \overline{X_k}$.

Other averages are the phasic average of ϕ, defined (Ishii 1975) by

$$\tilde{\phi}_k = \overline{X_k\phi}/\overline{X_k}, \tag{3}$$

and the mass-weighted average of ψ, defined (Ishii 1975) by

$$\hat{\psi}_k = \overline{X_k\rho\psi}/\overline{X_k\rho}, \tag{4}$$

where ρ is the density.

The time-averaged equations expressing the conservation of mass for phase k are (Ishii 1975)

$$\frac{\partial \alpha_k\tilde{\rho}_k}{\partial t} + \nabla.\alpha_k\tilde{\rho}_k\hat{\mathbf{v}}_k = \Gamma_k, \tag{5}$$

where $\hat{\mathbf{v}}_k$ is the mass-averaged velocity. The quantity Γ_k is (Ishii 1975) the rate of interfacial mass transfer to phase k:

$$\Gamma_k = -\sum_j \frac{1}{\mathbf{v}_1.\mathbf{n}_k\,T}\rho_k(\mathbf{v}_k-\mathbf{v}_1).\mathbf{n}_k, \tag{6}$$

where Σ_j indicates the summation over the discontinuities (interface passages) during the averaging interval T, $\mathbf{v}_1$ is interfacial velocity, $\mathbf{n}_k$ is the unit (outward) normal to phase k, and p_k and $\mathbf{v}_k$ are the values of the density and velocity on the phase-k side of the interface. Similarly, conservation of linear momentum for phase k is given by (Ishii 1975)

$$\begin{aligned}\alpha_k\tilde{\rho}_k(\partial\hat{\mathbf{v}}_k/\partial t + \hat{\mathbf{v}}_k.\nabla\hat{\mathbf{v}}_k) = {} & -\alpha_k\nabla\tilde{p}_k + \nabla.\alpha_k(\tilde{\boldsymbol{\tau}}_k + \tilde{\boldsymbol{\sigma}}_k) \\ & + \alpha_k\tilde{\rho}_k\mathbf{g}_k + (\tilde{p}_k - p_{k,1})\nabla\alpha_k + \mathbf{M}_k^{\mathrm{d}} + \Gamma_k(\hat{\mathbf{v}}_k - \mathbf{v}_{k,1}),\end{aligned} \tag{7}$$

where $\tilde{p}_k$ is the phasic-average pressure, $\tilde{\boldsymbol{\tau}}_k$ is the phasic average of the viscous stresses, $\boldsymbol{\sigma} = -X_k\rho(\mathbf{v}-\tilde{\mathbf{v}}_k)(\mathbf{v}-\tilde{\mathbf{v}}_k)$ is the 'turbulent' stress (due to velocity fluctuations about

the mass-weighted-average velocity), and $\mathbf{g}_k$ is the body force of phase k. Also, the rate of interfacial momentum transfer is written as

$$\mathbf{M}_k = \Gamma_k \mathbf{v}_{k,1} + p_{k,1}\nabla\alpha_k + \mathbf{M}_k^{\mathrm{d}} = -\sum_j \frac{1}{\mathbf{v}_1\cdot\mathbf{n}_k T}\rho_k \mathbf{v}_k(\mathbf{v}_k - \mathbf{v}_1)\cdot\mathbf{n}_k + \sum_j \frac{1}{\mathbf{v}_1\cdot\mathbf{n}_k T} p_{k,1}\mathbf{n}_k + \sum_j \frac{1}{\mathbf{v}_1\cdot\mathbf{n}_k T}[(p_k - p_{k,1})\mathbf{n}_k + \mathbf{n}_k\cdot\boldsymbol{\tau}_k], \quad (8)$$

where $\mathbf{v}_{k,1}$ and $p_{k,1}$ are respectively, the interfacial average velocity and pressure and p_k and $\boldsymbol{\tau}_k$ are the values of the pressure and the viscous stress on the phase-k side of the interface.

In (7), we have used the result that

$$\sum_j \frac{\mathbf{n}_k}{\mathbf{v}_1\cdot\mathbf{n}_k T} = -\nabla\alpha_k.$$

The detailed definitions and derivations of these equations can be found in Ishii's (1975) book.

In order to simplify the notation used in the remainder of this paper, we shall *drop all notation for averaging* (overbars etc.), except where such notation becomes unavoidable.

3. Void profile relations

It is our goal to examine the fundamental mechanisms governing phase distribution in pipe flows. Thus we shall restrict our attention to a special flow situation, namely the steady ($\partial/\partial t = 0$), fully developed ($\partial/\partial z = 0$, except for pressure) turbulent flow of an axisymmetric adiabatic air-water mixture in a circular vertical pipe. The assumption that the flow is steady and fully developed simplifies the mass- and momentum-balance equations immensely. Furthermore, treating an adiabatic air–water mixture obviates the need for considering the energy equation. Lastly, the assumption of axisymmetric flow in a circular pipe simplifies the geometry so that the problem becomes tractable.

It is convenient to neglect surface-tension effects and assume that $p_k = p_{k,1} = p$. Furthermore, we shall assume that both the liquid and gas phase densities are constant. This latter assumption is motivated by the observation that under normal conditions, the liquid and gas densities change very little. Moreover, the lateral phase distribution observed in solid–liquid systems indicates that compressibility effects cannot account completely for phase-distribution effects.

With these assumptions, we have $\alpha_k = \alpha_k(r)$, $\mathbf{v}_k = u_k(r)\mathbf{e}_z$, and $p = p(r,z)$. We denote gas by $k = \mathrm{G}$ and the liquid by $k = \mathrm{L}$. We also write $\alpha_{\mathrm{G}} = \alpha$, so that $\alpha_{\mathrm{L}} = 1-\alpha$. We see that the phasic equations of conservation of mass are satisfied identically; and the equations of momentum conservation become

$$0 = -\alpha\frac{\partial p}{\partial r} + \frac{d}{dr}(\alpha\sigma_{\mathrm{G},rr}) + \frac{1}{r}\alpha(\sigma_{\mathrm{G},rr} - \sigma_{\mathrm{G},\theta\theta}) \quad (9)$$

for conservation of gas momentum in the *radial direction*,

$$0 = -(1-\alpha)\frac{\partial p}{\partial r} + \frac{d}{dr}[(1-\alpha)\sigma_{\mathrm{L},rr}] + \frac{1}{r}(1-\alpha)(\sigma_{\mathrm{L},rr} - \sigma_{\mathrm{L},\theta\theta}) \quad (10)$$

for conservation of liquid momentum in the *radial direction*,

$$0 = -\alpha\frac{\partial p}{\partial z} - \alpha\rho_{\mathrm{G}} g\cos\theta + \frac{1}{r}\frac{d}{dr} r\alpha(\tau_{\mathrm{G},rz} + \sigma_{\mathrm{G},rz}) + M^{\mathrm{d}}_{\mathrm{G},z} \tag{11}$$

for conservation of gas momentum in the *axial direction*, and

$$0 = -(1-\alpha)\frac{\partial p}{\partial z} - (1-\alpha)\rho_{\mathrm{L}} g\cos\theta + \frac{1}{r}\frac{d}{dr} r(1-\alpha)(\tau_{\mathrm{L},rz} + \sigma_{\mathrm{L},rz}) - M^{\mathrm{d}}_{\mathrm{G},z} \tag{12}$$

for conservation of liquid momentum in the *axial direction*.

Our discussion is not too dependent on the particular form chosen for the interfacial momentum-transfer terms; however, for completeness we write

$$\begin{aligned} M^{\mathrm{d}}_{\mathrm{G},z} &= B^{M}(u_{\mathrm{L}} - u_{\mathrm{G}}) \\ &= \tfrac{3}{8}\alpha\rho_{\mathrm{L}}\frac{C_{\mathrm{D}}}{r_{\mathrm{b}}}|u_{\mathrm{L}} - u_{\mathrm{G}}|(u_{\mathrm{L}} - u_{\mathrm{G}}), \end{aligned}$$

where

$$C_{\mathrm{D}} = C_{\mathrm{D}}(Re_{\mathrm{b}}, \alpha).$$

The parameter r_{b} is the bubble radius, and C_{D} is the interfacial drag coefficient, which is assumed to depend on the bubble Reynolds number Re_{b} and the void fraction α. For bubbly air–water flows, one correlation that works reasonably well uses a standard low-Reynolds-number form, with a modified viscosity (Zuber & Ishii 1978)

$$C_{\mathrm{D}} = \frac{24}{Re_{\mathrm{b}}},$$

where

$$Re_{\mathrm{b}} = 2r_{\mathrm{b}}\rho_{\mathrm{L}}|u_{\mathrm{L}} - u_{\mathrm{G}}|/\mu_{\mathrm{m}},$$

and the effective mixture viscosity is taken to be,

$$\mu_{\mathrm{m}}/\mu_{\mathrm{L}} = \left(1 - \frac{\alpha}{\alpha_{\mathrm{Gm}}}\right)^{-2.5}\alpha_{\mathrm{Gm}}(\mu_{\mathrm{G}} + 0{\cdot}4\,\mu_{\mathrm{L}})/\mu_{\mathrm{G}} + \mu_{\mathrm{L}}),$$

where μ_{L} is the liquid viscosity and α_{Gm} is a constant. In (11) and (12), $\cos\theta = 1$ for upflow, and $\cos\theta = -1$ for downflow.

The pressure $p(r,z)$ can be separated as

$$p(r,z) = -\frac{\Delta p}{L}z + p'(r),$$

where $\Delta p = p_{\mathrm{i}} - p_{\mathrm{o}}$ is the pressure drop between the inlet and outlet of the pipe, and L is the length of the pipe. The function $p'(r)$ contains all information about the radial variations.

A relation between $\alpha(r)$ and the turbulence structure of the liquid has been derived, and the implications thereof explored in previous papers by Drew, Lahey & Sim (1978) and by Lahey & Drew (1979). These derivations will be summarized here to show the connection to the present work, and because it is convenient to use an intermediate result as a starting point for the present work.

The pressure gradient can be eliminated from (9) and (10). The resulting equation is

$$0 = \frac{d}{dr}(\alpha\sigma_{\mathrm{G},rr}) - \frac{\alpha}{1-\alpha}\frac{d}{dr}[(1-\alpha)\sigma_{\mathrm{L},rr}] + \frac{\alpha}{r}[(\sigma_{\mathrm{G},rr} - \sigma_{\mathrm{G},\theta\theta}) - (\sigma_{\mathrm{L},rr} - \sigma_{\mathrm{L},\theta\theta})]. \tag{13}$$

Serizawa's (1974) data shows that for bubbly flow the turbulent stress of the gaseous phase is proportional to that of the liquid phase. That is, we assume

$$\sigma_{G,ij} = (\rho_G/\rho_L)\, C_1 \sigma_{L,ij} = q\sigma_{L,ij}. \tag{14}$$

Equation (14) implies that the continuous (liquid) phase-velocity fluctuations drive the dispersed (gas) phase-velocity fluctuations.

We shall assume that q is not a function of r. Indeed, Serizawa's (1974) data indicates that $C_1 \simeq 1$ for bubbly flows. We see from (14) that $C_1 = 1$ implies that the r.m.s. velocity fluctuations of each phase are equal.

It is convenient to define

$$K_L = \tfrac{1}{2}\Sigma_i \sigma_{L,ii} = \tfrac{1}{2}\rho_L[(v'_{L,r})^2 + (v'_{L,\theta})^2 + (v'_{L,z})^2], \tag{15}$$

$$F_{jj} = \tfrac{1}{2}\sigma_{L,jj}/K_L \quad \text{(no summation on } j\text{)}. \tag{16}$$

K_L is the total turbulent kinetic energy of the liquid phase, and the 'F'-factors quantify the degree of anisotropy of turbulence structure.

After some manipulation, we obtain from (13)–(16),

$$\frac{d\alpha}{dr} = \frac{\alpha(1-\alpha)(1-q)}{\alpha+(1-\alpha)q}\left[\frac{d/dr\,(K_L F_{rr})}{K_L F_{rr}} - \frac{F_{\theta\theta}-F_{rr}}{rF_{rr}}\right]. \tag{17}$$

Equation (17) can be integrated to obtain

$$\frac{\alpha^q}{1-\alpha} = C_2(K_L F_{rr})^{1-q} \exp\left[-(1-q)\int_R^r \frac{F_{\theta\theta}(r')-F_{rr}(r')}{r' F_{rr}(r')}\, dr\right], \tag{18}$$

where C_2 is the constant of integration.

Equation (18) expresses a relation between the radial void fraction distribution $\alpha(r)$ and the liquid-phase turbulent-kinetic-energy distribution $K_L(r)$. Furthermore, the void distribution also depends on the anisotrophy of the liquid-phase turbulence.

Some aspects of the relationship between the local void fraction and the liquid-phase turbulence structure have been previously examined (Drew *et al.* 1978; Lahey & Drew 1979). It was found that the turbulence structure must lie between isotropic ($F_{rr} = F_{\theta\theta} = F_{zz} = \frac{1}{3}$), and the anisotropic structure found in single-phase turbulent flow in pipes. These works found it convenient to work with $K_{Lz} = K_L F_{zz}$, instead of K_L, since K_{Lz} is the quantity measured by Serizawa (1974).

Drew *et al.* (1978) show excellent agreement between the theory, (18) and the data of Serizawa (1974). Lahey & Drew (1979) have extended the derivation to ducts of arbitrary cross-section. However, since the void-fraction distribution is so dependent on the liquid-phase turbulence structure, it is desirable to derive a model which is more predictive. That is, we seek a model that requires less information about the turbulence structure to predict the lateral void profiles. Indeed this is the whole thrust of this paper.

4. Asymptotic analysis

For many flows of practical interest, we have $\rho_G/\rho_L \ll 1$, and thus q, defined in (14), is small. We wish to exploit the relative smallness of this parameter. If (11) and (12) are added, we can obtain the mixture momentum equation in the form

$$\frac{1}{r}\frac{d}{dr}r\{[\alpha\tau_{G,rz}+(1-\alpha)\tau_{L,rz}]+[\alpha\sigma_{G,rz}+(1-\alpha)\sigma_{L,rz}]\}$$
$$+\frac{\Delta p}{L}-[\alpha\rho_G+(1-\alpha)\rho_L]g\cos\theta=0. \tag{19}$$

If we neglect the ratio ρ_G/ρ_L compared to unity, (19) becomes

$$\frac{1}{r}\frac{d}{dr}r(1-\alpha)(\tau_{L,rz}+\sigma_{L,rz})+\frac{\Delta p}{L}-(1-\alpha)\rho_L g\cos\theta=0. \tag{20}$$

Furthermore, if we neglect ρ_G/ρ_L in (11), we have

$$\alpha\frac{\Delta p}{L}+B^M(u_L-u_G)=0. \tag{21}$$

Equation (21) expressed a balance between the interfacial drag force, and the pressure-gradient (buoyant) force. If $u_L(r)$ and $\alpha(r)$ are known, then (21) can be solved for $u_G(r)$.

We can view the roles of these equations in the following way. The radial momentum equations determine the phase distribution $\alpha(r)$ in terms of the liquid turbulence structure. Equation (18) expresses this result. The axial momentum equations, (11) and (12), reduce to (20) and (21) and yield the velocity fields, in terms of the imposed pressure gradient, and the void-fraction distribution $\alpha(r)$. Equation (21) can be solved for u_G, if u_L is known. Unfortunately, the turbulence structure is also involved in (18) and (20). Thus, (18) and (20) are coupled through the local void-fraction and turbulence terms. In order to proceed further, it is necessary to make some closure assumptions concerning the turbulence terms.

We have chosen a mixing-length theory for the closure relations for several reasons. First, for single-phase flow in a pipe, mixing length theory does a credible job in giving analytic results for the mean-flow properties, such as the velocity profile. Also, mixing-length theory is relatively simple and straightforward to apply. It is our opinion that a more complicated theory (such as a theory that predicts the kinetic energy) should be employed only after a simpler theory fails, or should be used to fill in details missed by the simpler theory. Note that an 'eddy-viscosity' theory, while simpler than mixing-length theory, is deficient in that it predicts $\sigma_{L,rr}=\sigma_{L,\theta\theta}=0$, which is not true for any but the most trivial two-phase flows. Finally, mixing-length theory allows us to model all components $\sigma_{L,ij}$, in accordance with the needs of (18) and (20).

Thus we write

$$\sigma_{L,rz}=\rho_L l_L^2\left|\frac{du_L}{dr}\right|\frac{du_L}{dr}, \tag{22}$$

where l_L is a mixing length.

We further assume that

$$K_{Lz}=K_L F_{ss}=\tfrac{1}{2}\rho_L\kappa_L^{-2}l_L^2\left(\frac{du_L}{dr}\right)^2+K_{L0}(r), \tag{23}$$

where κ_L is a constant. In (23), the term $K_{L0}(r)$ is added to the 'usual' mixing-length assumption for K_{Lz}, in order to overcome a classical difficulty with mixing-length theory at the centre-line. To understand this difficulty, consider (23) at the centre-line $r = 0$. At this location, $du_L/dr|_{r=0} = 0$, and $K_{Lz} = K_{L0}(0)$. Thus, without $K_{L0}(r)$, the turbulent kinetic energy at the centre-line would incorrectly be predicted to be zero. As we shall show shortly, the K_{L0} parameter is important in determining the void profile near the centre-line.

From (22) and (23), we have

$$\sigma_{L,rz} = -2\kappa_L^2 (K_{Lz} - K_{L0}) \tag{24}$$

where we have used $|du_L/dr| = -du_L/dr$, since we expect $du_L/dr < 0$. We shall further use a viscous model of the form

$$\tau_{L,rz} = \mu_L \frac{du_L}{dr}. \tag{25}$$

Combining (23) and (25) gives

$$\tau_{L,rz} = \frac{-\mu_L \kappa_L}{l_L} \left[\frac{2(K_{Lz} - K_{L0})}{\rho_L}\right]^{\frac{1}{2}}, \tag{26}$$

where the negative square root is chosen since

$$du_L/dr < 0.$$

Let us now examine (18), with the approximation that $q \ll 1$. This assumption implies that $1 - q = 1$; however, we must use caution with the quantity α^q. If α is not close to zero, we have

$$\alpha^q = e^{q \ln \alpha} = 1 + q \ln \alpha + \ldots. \tag{27}$$

If $\alpha = 0$, however, $\ln \alpha$ is not defined, and consequently the expansion (27) is not valid. To escape this difficulty, we shall leave α^q in (18), but use (27) when we know that $\alpha \neq 0$. Thus (18) gives

$$K_{Lz} = K_L F_{zz} = \frac{C_2^{-1} \alpha^q}{1 - \alpha} f(r), \tag{28}$$

where

$$f(r) = \frac{F_{zz}}{F_{rr}} \exp \int_R^r \frac{F_{\theta\theta}(r') - F_{rr}(r')}{r' F r r(r')} dr'. \tag{29}$$

Finally, combining (28), (29), (26) and (24) with (20), we obtain

$$-\frac{1}{r}\frac{d}{dr}\left\{\frac{r\mu_L \kappa_L}{l_L}\left[\frac{2\alpha^q C_2^{-1} f(r)/(1-\alpha) - K_{L0}}{\rho_L}\right]^{\frac{1}{2}} + 2r\kappa_L^2 [\alpha^q C_2^{-1} f(r) - K_{L0}(1-\alpha)]\right\}$$
$$+ \frac{\Delta p}{L} - (1-\alpha)\rho_L g \cos\theta = 0. \tag{30}$$

Equation (30) is an ordinary differential equation that governs the void profile $\alpha(r)$ throughout the cross-sectional area $0 \leqslant r \leqslant R$. The appropriate boundary conditions on $\alpha(r)$ are

$$\alpha(0) \quad \text{is bounded;} \tag{31a}$$

$$\alpha(R) = 0; \tag{31b}$$

$$\langle \alpha \rangle = \frac{1}{\pi R^2} \int_0^R 2\pi r \alpha(r) dr \quad \text{is given,} \tag{31c}$$

where $\langle\,\rangle$ denotes the cross-sectional average. Equation (31*b*) states that no vapour is in contact with the wall, and (31*c*) specifies the average void fraction in the pipe.

Equation (30) involves several parameters that characterize the turbulence structure; namely q, K_L, l_L, $f(r)$ and $K_{L0}(r)$. The present knowledge of two-phase turbulence modelling precludes the practical use of (30) for predicting the void profile. However, for many flows of practical interest, three conditions are satisfied; specifically

$$\rho_G/\rho_L \ll 1, \tag{32a}$$

$$Re_L = \frac{\rho_L U R}{\mu_L} \gg 1, \tag{32b}$$

$$|\sigma_{L,ij}| \ll \rho_L U^2, \tag{32c}$$

where U is a velocity scale. For example, in Serizawa's (1974) data, $\rho_G/\rho_L \simeq 0{\cdot}001$ and flow Reynolds numbers Re_L were greater than 10^5. Moreover, these data show that $\sigma_{L,zz}/\rho_L U^2 < 0{\cdot}1$ for all cases.

We wish to use these ideas to find approximate solutions of (30) valid in sub-regions of the interval $0 \leqslant r \leqslant R$. There are three sub-regions where meaningful approximate solutions can be found: near the wall, near the centre-line, and in the annular region between these regions. As we shall see, the above assumptions yield plausible approximate solutions of (30) that need little information about the turbulence structure.

Outer solution

Let us consider an approximation to (30) that is valid away from the wall. Near the wall, we expect viscous effects to be important. Away from the wall, however, we expect the viscous terms to be small compared with the turbulence terms. We also assume $\alpha^q \simeq 1$, since we don't expect α_0 to vanish. Away from the centre-line, we expect $K_{L0}(r) = 0$. Thus, the approximation valid away from the wall, and away from the centre-line is

$$-\frac{1}{r}\frac{d}{dr}[2r\kappa_L^2 \hat{C}_2^{-1} f(r)] + \frac{\Delta p}{L} - (1-\alpha_0)\rho_L g\cos\theta = 0. \tag{33}$$

Solving (33) for $\alpha_0(r)$ gives

$$\alpha_0(r) = 1 - \frac{\Delta p}{\rho_L g L\cos\theta} + \frac{1}{\rho_L g\cos\theta}\frac{1}{r}\frac{d}{dr}[2r\kappa_L^2 \hat{C}^{-1} f(r)]. \tag{34}$$

For low-quality bubbly flows we expect the pressure gradient and gravitational effects to dominate the turbulence effects. In this case, we have

$$\alpha_0(r) = 1 - \frac{\Delta p}{\rho_L g L\cos\theta}. \tag{35}$$

Thus in the 'outer' region α_0 is a constant. From figure 1, a constant α_0 is obviously a good approximation for low-quality bubbly co-current flows.

The appearance of the pressure drop Δp in (35) is inconvenient for some of the calculations in subsequent sections. For that reason, we shall eliminate the pressure drop from (35) using the area-averaged pressure-drop equation. To obtain this equation, let us now multiply (20) by $2\pi r$, and integrate from $r = 0$ to $r = R$. This yields

$$2\pi R(1-\alpha(R))\tau_{L,rz}(R) + \pi R^2\frac{\Delta p}{L} - \pi R^2(1-\langle\alpha\rangle)\rho_L g\cos\theta = 0, \tag{36}$$

where

$$\langle\alpha\rangle = \frac{1}{\pi R^2}\int_0^R 2\pi r\alpha(r)\,dr, \tag{37}$$

and we have assumed that $\sigma_{L,rz} = 0$ at $r = R$. From (18), we note that since $K_L = 0$ at $r = R$, we must have $\alpha(R) = 0$. Thus (36) becomes

$$\frac{2\tau_{L,rz}(R)}{R} + \frac{\Delta p}{L} - (1-\langle\alpha\rangle)\rho_L g\cos\theta = 0. \tag{38}$$

We further note that $\tau_{L,rz}(R)$ is the force per unit area exerted by the fluid on the pipe wall. Thus we write $\tau_{L,rz}(R) = -\tau_w$, where τ_w is the force per unit area exerted on the fluid by the pipe. From (38) we have

$$-\frac{2\tau_w}{R} + \frac{\Delta p}{L} - (1-\langle\alpha\rangle)\rho_L g\cos\theta = 0. \tag{39}$$

The pressure gradient $\Delta p/L$ can be eliminated from (35), resulting in

$$\alpha_0(r) = \langle\alpha\rangle - \frac{2\tau_w}{\rho_L g R\cos\theta}. \tag{40}$$

Let us now seek an approximate 'inner' solution valid near the centre-line.

Inner (Centre-line) solution

First, we can rescale the radial co-ordinate by letting $r = \epsilon\gamma$, where ϵ is to be chosen to balance the first derivatives in (30) with the wall-shear and gravitational terms. The desired balance can be achieved by choosing

$$\epsilon = \frac{2\kappa_L^2 K_{L0}(0)}{\rho_L g}.$$

We shall further assume that $\alpha^q \simeq 1$. From (28), we note that for $r = 0$ and $q \ll 1$,

$$C_2^{-1} f(0) = [1-\alpha(0)]\,K_{Lz}(0). \tag{41}$$

Since $K_{Lz}(0) = K_{L0}(0)$, (30) becomes, to lowest order

$$-\frac{1}{\gamma}\frac{d}{d\gamma}(1-\alpha(0))\gamma + \frac{1}{\gamma}\frac{d}{d\gamma}\gamma(1-\alpha) + \frac{2\tau_w}{\rho_L g R} + (\alpha-\langle\alpha\rangle)\cos\theta = 0. \tag{42}$$

The wall stress can be eliminated through (40), giving

$$\frac{d}{d\gamma}[\gamma(1-\alpha)] = 1-\alpha(0) - \gamma(\alpha-\alpha_0)\cos\theta. \tag{43}$$

The solution of (43) is

$$\alpha(\gamma) = \alpha_0 - \frac{Ce^{\cos\theta\gamma}}{\gamma} - \frac{\alpha(0)-\alpha_0}{\gamma\cos\theta}, \tag{44}$$

where C is the constant of integration.

Let us now consider the upflow ($\cos\theta = 1$) and downflow ($\cos\theta = -1$) cases separately.

Upflow ($\cos\theta = 1$) *case*. In order to match $\alpha(\gamma)$ to α_0 as $\gamma \to \infty$, we must have $C = 0$.

Furthermore, for $\alpha(0)$ to be finite, we must also have $\alpha(0) = \alpha_0$. Therefore, the 'inner solution' for the centre-line approximation becomes

$$\alpha(r) = \alpha_0. \tag{45}$$

That is, for upflow there is no perceptible build-up of void at the centre-line.

Downflow ($\cos\theta = -1$) *case*. Here C is *not* determined by matching as $\gamma \to \infty$; in fact $\alpha \to \alpha_0$ as $\gamma \to \infty$. For $\alpha(0)$ to be bounded, we must have $\alpha(\gamma)$ finite as $\gamma \to 0$. This implies the requirement

$$C = \alpha(0) - \alpha_0,$$

so that

$$\alpha(\gamma) = \alpha_0 + \frac{\alpha(0)-\alpha_0}{\gamma}[1-e^{-\gamma}]. \tag{46}$$

In this case, however, requiring boundness at $\gamma = 0$ gives no further restrictions on the parameters. Hence, for downflow $\alpha(0)$ is arbitrary, and must be specified by some other means.

Thus the amount of vapour in the centre-line region for upflow is determined through matching. For downflow, on the other hand, the void profile has a degree of freedom, which means that the amount of vapour in the centre-line region is still to be determined. This problem will be resolved when the full solution is discussed.

Let us now consider the 'inner' solution valid near the pipe wall.

Inner (Wall) solution

Since we are looking for a valid approximation near the wall, it is convenient to define

$$R - r = \epsilon^* \zeta, \tag{47}$$

where the small parameter ϵ^* will be chosen to balance the terms in (30) involving $d\alpha/dr$ and the pressure gradient. As will be shown, this choice of ϵ^* will allow us to satisfy the wall boundary condition $\alpha(R) = 0$.

Let us also assume that near the wall the mixing length can be written as

$$l_{\mathrm{L}}(r) = k_{\mathrm{L}}(R-r) = k_{\mathrm{L}}\epsilon^*\zeta. \tag{48}$$

In order to balance the terms involving $d\alpha/dr$ and $\Delta p/L$ in (30), the correct choice of the parameter ϵ^* is

$$\epsilon^{*2} = \frac{\mu_{\mathrm{L}}\kappa_{\mathrm{L}}}{2k_{\mathrm{L}}\rho_{\mathrm{L}}g}\left[\frac{2C_2^{-1}f(R)}{\rho_{\mathrm{L}}}\right]^{\frac{1}{2}}. \tag{49}$$

Dividing (30) through by $\rho_{\mathrm{L}}g$, using (49), and neglecting terms of order ϵ^*, we obtain

$$-\frac{(1-\alpha)^{\frac{1}{2}}\alpha^{\frac{1}{2}q}}{\zeta}\left[\frac{1}{(1-\alpha)}-\frac{q}{\alpha}\right]\frac{d\alpha}{d\zeta} + A\alpha^{q-1}\frac{d\alpha}{d\zeta} - 2\frac{(1-\alpha)^{\frac{1}{2}}\alpha^{\frac{1}{2}q}}{\zeta^2} + B + \alpha\cos\theta = 0, \tag{50}$$

where

$$A = \frac{2\kappa_{\mathrm{L}}^2 C_2^{-1}f(R)}{\rho_{\mathrm{L}}g}\left(\frac{q}{\epsilon^*}\right), \tag{51}$$

$$B = \frac{1}{\rho_{\mathrm{L}}g}\left\{\frac{\Delta p}{L} - \rho_{\mathrm{L}}g\cos\theta - \frac{2\kappa_{\mathrm{L}}^2 C_2^{-1}\alpha^q}{R}\left[f(R) - R\frac{df(R)}{dr}\right]\right\}. \tag{52}$$

We note that away from the centre-line of the pipe, $K_{\mathrm{L}0} = 0$. Since under atmospheric

conditions $q \ll 1$, we have $\alpha^q \simeq 1$. However, we do not neglect A, since it is proportional to q/ϵ^*, and ϵ^* is also a small parameter.

Let us now consider the parameter B. For the case in which $q \ll 1$,

$$B = \frac{1}{\rho_L g}\left\{\frac{\Delta p}{L} - \rho_L g \cos\theta - \frac{2\kappa_L^2 C_2^{-1}}{R}\left[f(R) - R\frac{df(R)}{dr}\right]\right\}. \tag{53}$$

It is convenient to write the parameter B in terms of 'outer-solution' quantities. If we examine (34), we see that

$$B = -\alpha_0(R)\cos\theta. \tag{54}$$

If we further use (54) in (50) we have

$$\frac{d\alpha}{d\zeta} = \frac{2\zeta^{-2}(1-\alpha)^{\frac{1}{2}} - [\alpha - \alpha_0(R)]\cos\theta}{A\alpha^{-1} - \zeta^{-1}(1-\alpha)^{-\frac{1}{2}}}. \tag{55}$$

The appropriate boundary condition for (55) is

$$\alpha(0) = 0. \tag{56}$$

In addition, we must satisfy a matching condition (to merge the inner and outer solutions) given by

$$\lim_{\zeta\to\infty} \alpha(\zeta) = \alpha_0(R). \tag{57}$$

Equation (55) governs the void profile near the wall. It does not appear to be possible to achieve a closed-form quadrature of (55); however, important information about its solution can be obtained through the use of graphical techniques. To do this, let us divide the region of interest into regions where $d\alpha/d\zeta > 0$ and $d\alpha/d\zeta < 0$.

We note in (55) that $d\alpha/d\zeta = 0$ when the numerator is zero (unless the denominator is also zero), that is $d\alpha/d\zeta = 0$ when

$$N = \frac{2(1-\alpha)^{\frac{1}{2}}}{\zeta^2} - [\alpha - \alpha_0(R)]\cos\theta = 0. \tag{58}$$

For the cases of interest here, $\cos\theta = +1$ for upflow and $\cos\theta = -1$ for downflow. The curve in the (α, ζ)-plane along which $d\alpha/d\zeta = 0$ is given by (58) as

$$\alpha = \alpha_0(R) - \frac{2}{\zeta^4} \pm \frac{2}{\zeta^2}(1/\zeta^4 + 1 - \alpha_0(R))^{\frac{1}{2}}, \tag{59}$$

where the plus sign is for upflow and the negative sign is for downflow.

It is also interesting to consider the curve along which the denominator of (55) vanishes. This is given by the solution of the equation

$$D = A\alpha^{-1} - \zeta^{-1}(1-\alpha)^{-\frac{1}{2}} = 0, \tag{60}$$

which is

$$\alpha = -\tfrac{1}{2}(A\zeta)^2 + \tfrac{1}{2}(A\zeta)^2[1 + 4A^{-2}\zeta^{-2}]^{\frac{1}{2}}. \tag{61}$$

The curves in the (α,ζ)-plane where the numerator and the denominator are equal to zero are shown in figures 2 and 3 for upflow and downflow respectively. Typical solution curves (of (55)) are also shown. These curves were drawn by considering the slope $d\alpha/d\zeta$, and noting that the solution curve cannot cross the denominator-equals-zero curve (61), except possibly where there is an intersection with the numerator-equals-zero curve (59). This latter situation cannot occur, since if the solution curve had gone

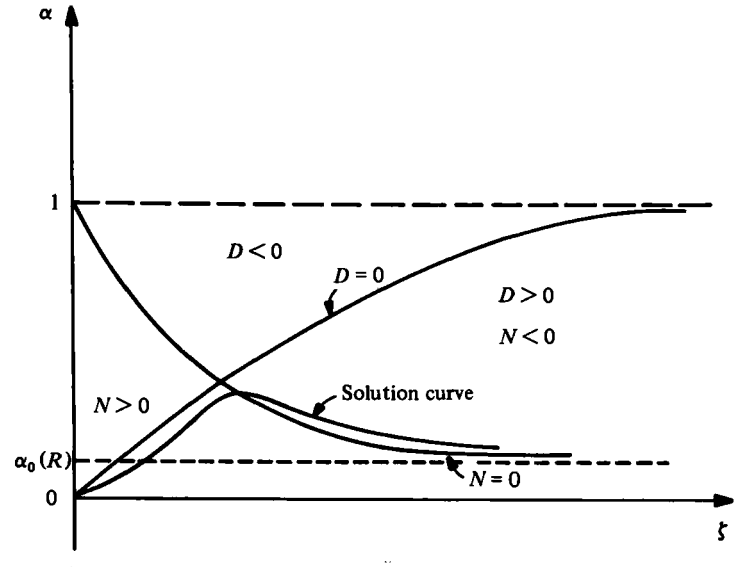

FIGURE 2. α *vs.* ζ for upflow ($\cos\theta = +1$). N is numerator of (69); D is denominator of (71); $d\alpha/d\zeta = N/D$.

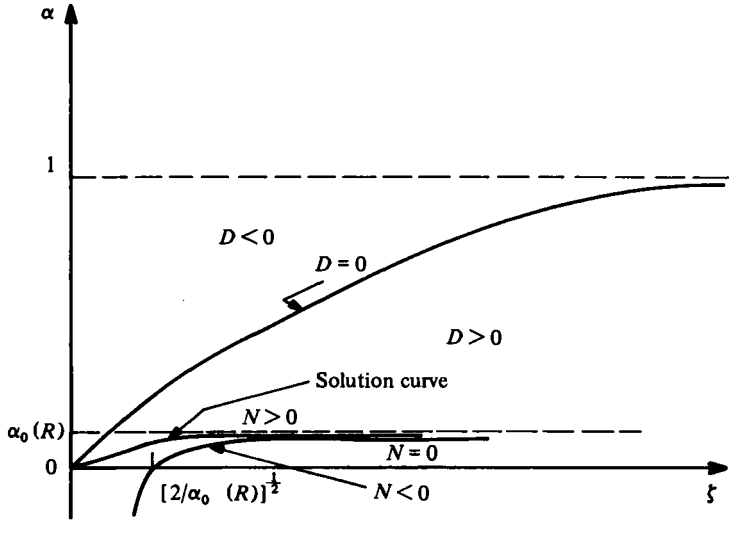

FIGURE 3. α *vs.* ζ for downflow ($\cos\theta = -1$).

through the intersection point it would be in a region where $N < 0$ and $D < 0$, thus $d\alpha/d\zeta = N/D > 0$, and it could never return to the $\alpha_0(R)$ line.

It is interesting to note that for the upflow case there is peaking of the void fraction in the wall region, while for the downflow case no peaking is predicted. This is exactly the trend seen in the data of Oshinowo & Charles (1974). Thus it appears that both the inner and outer solution correctly predict the observed 'bubble-coring' trends.

Matching

Let us now put these solutions together. There are three pieces, given respectively by (40) for the 'outer' region, away from the walls and centre-line; (55) for the 'inner'

solution of the wall layer; and (45) and (46), which are the 'inner' solutions valid near the centre-line.

In order to appreciate the relationship between these results, we must first note one feature of the solutions of (55). For upflow, there are many possible 'inner' solutions that are valid near the wall layer. This non-uniqueness is due to the singularity at the origin. It can also be seen by looking at figure 2. The solution curve shown is only one of many possible solution curves. Others may be obtained in the following way. On the curve $N = 0$ select a point that is below the intersection of the $N = 0$ and $D = 0$ curves. Integrate (55) back to $\zeta = 0$, and forward to $\zeta = \infty$. This gives a solution to (55) that satisfies $\alpha(0) = 0$ and $\alpha \to \alpha_0(R)$ as $\zeta \to \infty$. For each point selected on the curve $N = 0$ there is a solution.

As discussed previously, we also see in (46) the same sort of non-uniqueness in the centre-line approximation for downflow. That is, any choice of $\alpha(0)$ gives a valid solution. In contrast, as can be seen in figure 2, for the downflow case, the 'inner' (wall-layer) solution to (55) is unique.

The total picture, then, must be as follows. First, for upflow, the overall solution is as shown in figure 4. Note that there is no singular behaviour at the centre-line. The particular wall-layer solution must be chosen to satisfy the necessary condition that

$$\langle \alpha \rangle = \int_0^R \alpha(r) 2\pi r \, dr / \pi R^2.$$

For the downflow, the overall solution is as shown in figure 5. There are separate 'boundary' layers at the wall and at the centre-line of the pipe. The wall-layer solution is uniquely determined, but the centre-line solution is not. Here, the particular centre-line solution must be chosen to satisfy the necessary condition that

$$\langle \alpha \rangle = \int_0^R \alpha(r) 2\pi r \, dr / \pi R^2.$$

5. Discussion

For low-quality bubbly flow we have been able to construct appropriate 'inner' and 'outer' solutions that require little information about the turbulence structure and yet predict properly the observed effect of the flow orientation.

There are numerous assumptions involved in the solutions presented here. To aid the reader in assessing these assumptions, we shall recap them here.

The flow is assumed to be steady, fully-developed, adiabatic air–water bubbly flow. Surface tension is assumed to be negligible, and the phasic pressures are assumed to be equal.

Several assumptions have been made concerning the turbulent stresses. First, the gas-phase turbulence-stress tensor is assumed to be proportional to the liquid-phase stress tensor, the constant of proportionability being proportional to ρ_G/ρ_L (see (14)). Mixing-length theory is used to model the liquid-phase turbulent stresses. In accordance with standard practice, the mixing length is assumed proportional to the distance from the wall, in the region near the wall. With these assumptions, it is shown that void profile $\alpha(r)$ obeys (30), with the laminar and Reynolds stresses given respectively by (24) and (26). The relation between the liquid turbulent kinetic energy and the void fraction is given by (28).

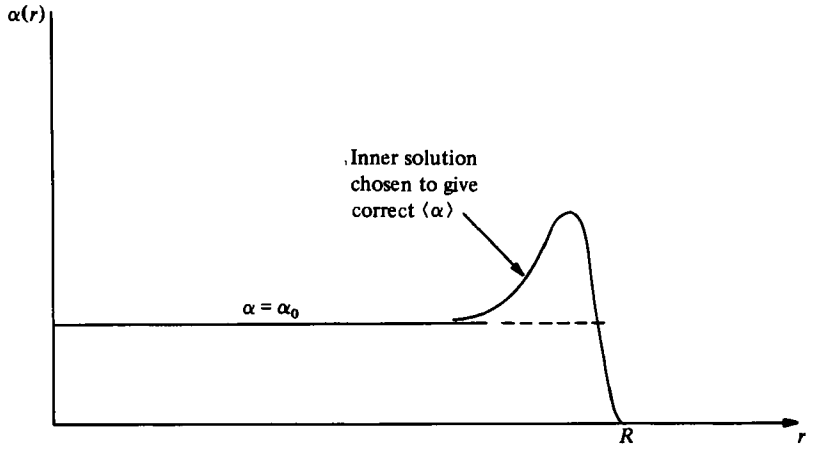

FIGURE 4. Theoretical solution – low-quality, bubbly upflow.

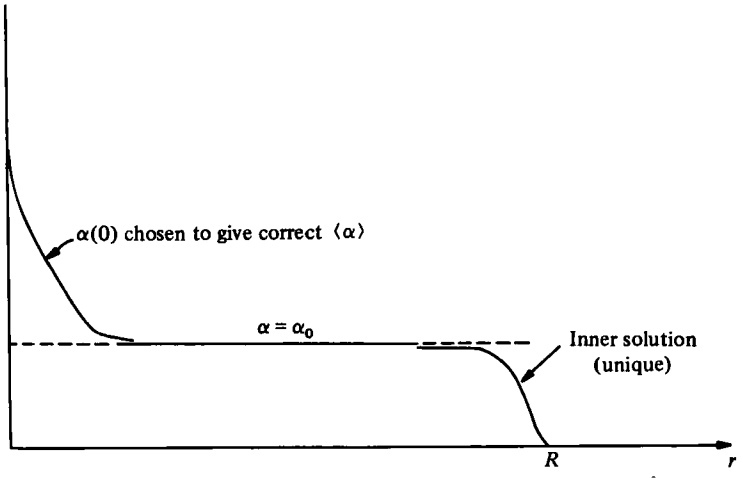

FIGURE 5. Theoretical solution – low-quality, bubbly downflow.

Next, three physical assumptions were made. First, the gas density was assumed to be small compared to the liquid density. The flow Reynolds number was assumed to be large, and the r.m.s. liquid turbulent-velocity fluctuations were assumed to be small compared to the mean-flow velocity.

With these assumptions, the pipe cross-section breaks up naturally into the flow near the wall, and the flow in the core region, away from the wall. The flow in the wall boundary layer is governed by (55), which quantifies the balance between the pressure drop and gravitational force, the viscous stress, and the Reynolds stress, where the mixing length is assumed to be proportional to the distance from the wall.

In the core, except near the centre-line, where mixing-length theory is inadequate, the void fraction is constant, and is given by (40). The balance in the core, except near the centre-line, is between the pressure gradient and the gravitational force. Near the centre-line, the classical mixing-length model was modified, yielding the void profile given by (44). This equation represents the balance between the pressure drop,

gravitational force and the Reynolds stress. This solution for void fraction is constant for upflow, and shows a peak at the centre for downflow.

For low-quality bubbly flow, the void profile $\alpha(r)$ is determined by competing mechanical effects, and is quite different for upflow and downflow. We have been able to construct approximate (inner and outer) solutions that predict these observed effects.

If the turbulence level is negligible compared with the imposed pressure gradient, then the 'outer' flow (i.e. the flow in the region between the wall and the centre-line) has a uniform void distribution. Near the wall, the interaction of turbulent stresses and viscous stresses determine the void distribution. For upflow, these forces combine to give a peak in the void profile near the wall.

Such a bubble layer is not found near the wall for downflow. Rather, a peak in the void profile is found at the centre-line for downflow. The height of these void peaks, which occur at different places for the two different flows, depends on the amount of vapour in the pipe. For upflow, the 'outer' flow has a certain amount of vapour flow area associated with it. Normally, this is not equal to $\langle\alpha\rangle\pi R^2$. From (40), we note that $\alpha_0 < \langle\alpha\rangle$, since there is appreciable vapour in the wall's bubble layer. For downflow, the 'outer flow' again contains a certain amount of vapour. From (40), we again note that $\alpha_0 < \langle\alpha\rangle$, where the excess vapour is now in the core (i.e. centre-line) region.

It is clear that the analysis present herein has captured the essential physics involved in the radial phase-separation process for bubbly flow. It should also be clear that considerably more work remains to be done to understand the turbulence structure if $\alpha(r)$ predictions are desired for more complex cases, such as churn-turbulent two-phase flows.

This research was supported by the United States Nuclear Regulatory Commission under contract NRC-04-76-301. This support is gratefully acknowledged.

REFERENCES

Delhaye, J. M. 1968 Equations fondamentals des écoulments diphasiques. CEA-R-3429.

Drew, D. A., Lahey, R. T. & Sim, S. 1978 Radial phase-distribution mechanisms in two-phase flow. In *Proc. OECD (NEA) CSNI Sec. Specialists Meeting on Transient Two-Phase Flow; Paris, June* 1978, *CSNI Rep.* no. 31.

Ishii, M. 1975 *Thermo-Fluid Dynamic Theory of Two-Phase Flow.* Eyrolles.

Lahey, R. T. & Drew, D. A. 1979 The analysis of phase distribution in fully developed two-phase flows. In *Proc. 2nd Multi-Phase Flow and Heat Transfer Symp.–Workshop.* Hemisphere.

Oshinowo, T. & Charles, M. E. 1974 Vertical two-phase flow, Part 1, flow pattern correlations. *Can. J. Ch. Engng* **52**, 25–35.

Serizawa, A. 1974 Fluid dynamic characteristics of two-phase flow. Ph.D. Thesis, Kyoto University, Japan.

Zuber, N. & Ishii, M. 1978 Relative motion and interfacial drag coefficient in dispersed two-phase flow of bubbles, drops and particles. In *Proc. 71st Ann. Meeting, Miami, A.I.Ch.E. Paper* no. 56a.